ISSN: 3064-6758 www.aristonpubs.com/sciengg-advances https://doi.org/10.69626/sea.2025.0059

RESEARCH ARTICLE

Synthesis, Characterization, and Multifunctional Applications of Graphene Oxide Quantum Dots in Environmental Remediation and Biomedical Drug Delivery

M. Beaula Ruby Kamalam*, K. J. Sam Daniel, K. Hariramakrishnan, L. Ganesh, S. S. R. Inbanathan

ABSTRACT: This study presents the synthesis and comprehensive characterization of graphene oxide quantum dots (GOQDs) for applications in environmental remediation and biomedical drug delivery. Graphite oxide was initially synthesized using the modified Hummers method, followed by exfoliation via ultrasonication to obtain graphene oxide (GO). The GO was subsequently converted into GOQDs through hydrothermal treatment, yielding nanoparticles with enhanced optical and catalytic properties. The structural, chemical, and optical characteristics of GOQDs were systematically analyzed using UV-Vis spectroscopy, photoluminescence (PL), X-ray diffraction (XRD), and Fourier-transform infrared (FTIR) spectroscopy. The results confirmed the successful formation of GOQDs with distinct absorption and emission properties, making them suitable for photocatalytic applications. In environmental remediation, GOQDs demonstrated high efficiency in the degradation of methylene blue dye, achieving a degradation rate of 94.51% under UV irradiation, highlighting their potential for wastewater treatment. For biomedical applications, GOQDs were functionalized with polyethylene glycol (PEG) to enhance their biocompatibility and stability. Hemolytic assays and MTT cytotoxicity tests confirmed their low toxicity and suitability for drug delivery systems. Furthermore, drug loading studies using tetracycline revealed a high drug loading efficiency (DLE) of 95.8% and a drug loading content (DLC) of 1.23%, underscoring their potential as nanocarriers for targeted drug delivery. This research underscores the versatility of GOQDs, demonstrating their dual functionality in environmental catalysis and biomedical applications. The findings provide a foundation for future studies on optimizing GOQD-based systems for industrial and therapeutic uses.

Keywords: Graphene oxide quantum dots (GOQDs), Hydrothermal synthesis, Photocatalytic degradation, Drug delivery, Biocompatibility, Methylene blue degradation.

Received: 20 October 2024; Revised: 19 December 20xx; Accepted: 15 January 2025; Available Online: 26 January 2025

1. INTRODUCTION

Nanomaterials have revolutionized modern science and technology, opening new frontiers in environmental research, electronics, and medicine [1]. These materials, typically with at least one dimension in the nanoscale range (1–100 nm), exhibit unique properties due to their high surface area-to-volume ratio and quantum confinement effects [2]. Unlike their bulk counterparts, nanomaterials demonstrate enhanced electrical, optical, and mechanical characteristics, leading to superior reactivity, catalytic efficiency, and novel behaviors that are unattainable at larger scales [3]. Among these nanomaterials, graphene oxide quantum dots (GOQDs) have garnered significant attention due to their exceptional physicochemical properties and versatile applications in environmental remediation and biomedicine [4].

Graphene oxide (GO), a two-dimensional carbon-based

Department of Physics, The American College, Madurai-625002, India

*Author to whom correspondence should be addressed: bealthambu10@gmail.com (M. Beaula Ruby Kamalam)

material composed of a hexagonal lattice of carbon atoms, is decorated with oxygen-containing functional groups such as carboxyl, epoxy, and hydroxyl groups [5]. These functional groups impart high chemical reactivity to GO, making it an adaptable platform for nanomaterial synthesis and functionalization [6]. However, when GO is reduced to the nanoscale (2–10 nm) to form quantum dots, its electronic and optical properties undergo dramatic changes due to quantum confinement effects [7]. Graphene oxide quantum dots (GOQDs) exhibit size-dependent photoluminescence (PL), tunable bandgaps, and enhanced catalytic activity, distinguishing them from bulk graphene oxide [8]. These properties make GOQDs highly suitable for applications in biosensing, bioimaging, drug delivery, and environmental catalysis [9].

The transition from graphene oxide to quantum dots offers several advantages, including improved photoluminescence, increased surface area, and superior catalytic performance [10]. The tunable PL of GOQDs, influenced by their size and surface functionalization, enables their use in fluorescence-based biological imaging and sensing [11]. Additionally, their large surface area and abundant oxygen-containing groups facilitate efficient drug loading and pollutant adsorption, making them ideal for biomedical and environmental applications [12]. In drug delivery, GOQDs can be functionalized with biomolecules such as polyethylene glycol (PEG) to enhance their solubility, stability, and biocompatibility [13]. PEGylation reduces aggregation and minimizes cytotoxicity, making GOQDs safe for in vivo applications [14]. Furthermore, their ability to encapsulate therapeutic agents via π-π stacking, electrostatic interactions, and hydrogen bonding allows for controlled drug release and targeted delivery [15].

The synthesis of GOQDs typically involves the fragmentation of graphene oxide sheets through chemical, physical, or hydrothermal methods [16]. Among these, the hydrothermal approach is widely preferred due to its simplicity, cost-effectiveness, and ability to produce GOQDs with a controlled size distribution [17]. In this method, GO is subjected to high temperature and pressure in a sealed autoclave, leading to its reduction and fragmentation into quantum dots [18]. The resulting GOQDs exhibit distinct optical and electronic properties, which can be fine-tuned by adjusting synthesis parameters such as temperature, reaction time, and precursor concentration [19].

Characterization of GOQDs is essential to understand their structural and functional properties. Techniques such as UV-Vis spectroscopy provide insights into their optical absorption and electronic transitions, while photoluminescence (PL) spectroscopy reveals their emission characteristics [20]. X-ray diffraction (XRD) analysis confirms the crystalline or amorphous nature of GOQDs, and Fourier-transform infrared (FTIR) spectroscopy identifies their surface functional groups [21]. These characterization techniques collectively help optimize GOQD synthesis for specific applications, ensuring high performance in catalysis, sensing, and drug delivery [22].

In biomedicine, GOQDs have shown immense potential as nanocarriers for drug delivery due to their high drug-loading capacity and biocompatibility [23]. Studies have demonstrated their efficacy in delivering chemotherapeutic agents, antibiotics, and nucleic acids, with enhanced targeting and reduced side effects [24]. For instance, PEGylated GOQDs loaded with tetracycline exhibit high drug-loading efficiency (95.8%) and sustained release, making them promising candidates for antibacterial therapy [25]. Additionally, their low cytotoxicity, as confirmed by hemolytic assays and MTT tests, ensures their safety for therapeutic use [26].

In environmental applications, GOQDs serve as efficient photocatalysts for degrading organic pollutants such as methylene blue, achieving degradation efficiencies exceeding 94% under UV irradiation [27]. Their high surface area and reactive oxygen groups enable effective adsorption and catalytic breakdown of dyes, heavy metals, and pharmaceutical waste [28]. The incorporation of GOQDs into wastewater treatment systems could provide a sustainable solution for industrial effluent purification [29].

Despite their promising attributes, challenges remain in scaling up GOQD production and ensuring long-term stability in biological and environmental systems [30]. Future research should focus on optimizing synthesis protocols, exploring novel functionalization strategies, and conducting in-depth toxicological studies to facilitate their commercialization and clinical translation.

2. EXPERIMENTAL DETAILS

2.1. Synthesis of Graphite Oxide via Modified Hummers Method

The synthesis of graphite oxide was carried out using the modified Hummers method, which involves the oxidation of graphite powder in the presence of strong oxidizing agents. In a typical procedure, 48 mL of concentrated sulfuric acid (H_2SO_4, 98%) was added to a 1-liter round-bottom flask placed in an ice bath to maintain a low temperature (0–5°C). Under continuous stirring, 2 grams of graphite powder (purity >99%) and 6 grams of potassium permanganate ($KMnO_4$) were slowly added to the acid solution in small increments to prevent excessive heat generation and potential explosion risks. The mixture was stirred vigorously for 2 hours to ensure complete oxidation of graphite.

After the initial reaction, 150 mL of double-distilled (DD) water was gradually added to the flask under constant stirring, causing the temperature to rise to approximately 98°C. The solution turned brown, indicating the formation of graphene oxide. To terminate the oxidation process, 8 mL of hydrogen peroxide (H_2O_2, 30%) and 280 mL of DD water were introduced, resulting in a color change to bright yellow, confirming the successful synthesis of graphite oxide. The mixture was then stirred for an additional 12 hours to ensure complete reaction and stabilization.

To remove residual metallic ions and unreacted graphite,

the solution was treated with 3% hydrochloric acid (HCl) and centrifuged at 5000 rpm for 15 minutes. The supernatant was discarded, and the remaining solid was washed repeatedly with DD water until the pH reached neutral (pH ≈ 7). The purified graphite oxide slurry was collected via vacuum filtration using Whatman filter paper (pore size 0.45 µm) and dried in an air oven at 60°C for 2 hours to obtain the final graphite oxide powder.

2.2. Exfoliation of Graphene Oxide (GO) via Ultrasonication

The synthesized graphite oxide was exfoliated into graphene oxide (GO) nanosheets using a high-intensity ultrasonic probe. A dispersion was prepared by adding 2 mg/mL of graphite oxide to DD water, followed by magnetic stirring for 30 minutes to ensure uniform mixing. The solution was then subjected to probe sonication (20 kHz, 750 W) for 3 hours in an ice bath to prevent overheating. The ultrasonic waves induced cavitation, breaking the interlayer van der Waals forces and yielding thin GO nanosheets. After sonication, the dispersion was centrifuged at 5000 rpm for 30 minutes to remove any unexfoliated graphite oxide aggregates. The supernatant, containing well-dispersed GO nanosheets, was collected, while the sediment was discarded. The GO suspension was dried at 60°C for 2 hours to obtain a powdered form, which was stored in an airtight container to prevent moisture absorption and oxidation.

2.3. Synthesis of Graphene Oxide Quantum Dots (GOQDs) via Hydrothermal Treatment

The GOQDs were synthesized using a hydrothermal method, which facilitates the controlled fragmentation of GO sheets into quantum dots. A homogeneous GO dispersion (1 mg/mL in DD water) was prepared by stirring for 30 minutes, followed by bath sonication for 1 hour to ensure complete exfoliation. The solution was then transferred into a 100 mL Teflon-lined stainless-steel autoclave and heated at 160°C for 12 hours. Under high temperature and pressure, the GO sheets underwent reduction and fragmentation, forming small-sized quantum dots with enhanced photoluminescence properties.

After cooling to room temperature, the resulting GOQD solution was centrifuged at 10,000 rpm for 20 minutes to remove any large particles or aggregates. The supernatant was collected and dried in an air oven at 60°C to obtain a solid GOQD powder. The powder was finely ground using an agate mortar and pestle and stored in a dark, airtight container to prevent photodegradation.

2.4. Characterization of GO and GOQDs

The optical properties of GO and GOQDs were analyzed using a UV-Vis spectrophotometer (Shimadzu UV-2600). The samples were dispersed in DD water (0.01 mg/mL), and absorbance spectra were recorded in the range of 200–800 nm. GO exhibited characteristic absorption peaks at 236 nm (π–π^* transitions of C=C bonds) and a shoulder at 368 nm (n–π^* transitions of C=O groups). In contrast, GOQDs showed a strong absorption peak at 200–230 nm, indicating quantum confinement effects. The fluorescence properties of GO and GOQDs were studied using a fluorescence spectrometer (Horiba Fluoromax-4). The excitation wavelength was set at 320 nm, and emission spectra were recorded from 350–600 nm. GO exhibited weak fluorescence at 398 nm, while GOQDs displayed strong emission at 432 nm due to quantum confinement and edge effects. FTIR analysis (PerkinElmer Spectrum Two) was performed to identify functional groups. GO showed peaks at 3413 cm^{-1} (O-H stretching), 1590 cm^{-1} (C=C stretching), and 1058 cm^{-1} (C-O stretching). After hydrothermal treatment, GOQDs exhibited reduced oxygen-containing groups, confirming partial reduction. XRD (Bruker D8 Advance) analysis was conducted using Cu-Kα radiation (λ = 1.5406 Å). GO showed a sharp peak at 2θ ≈ 10.5°, corresponding to the (001) plane. GOQDs exhibited a broad peak at 2θ ≈ 21°, indicating an amorphous structure. The crystallite size was calculated using the Scherrer equation ($D = K\lambda/\beta\cos\theta$), yielding an average size of 9.77 nm. SEM (Hitachi SU-70) was used to examine the morphology of GO and GOQDs. GO appeared as wrinkled sheets, while GOQDs exhibited spherical nanoparticles with uniform dispersion.

2.5. Photocatalytic Dye Degradation Study

A stock solution of MB (10 ppm) was prepared by dissolving 10 mg of MB dye in 1 liter of DD water. For degradation studies, 30 mL of MB solution was diluted with 70 mL of DD water to obtain a 3 ppm solution. 10 mg of GOQDs were added to 100 mL of the MB solution (3 ppm) and stirred in the dark for 30 minutes to establish adsorption-desorption equilibrium. The mixture was then exposed to UV light (365 nm, 125 W) with continuous stirring. Aliquots (3 mL) were collected at 30-minute intervals and centrifuged to remove GOQDs. The supernatant was analyzed using UV-Vis spectroscopy to monitor MB degradation by measuring absorbance at 664 nm. The degradation efficiency was calculated using the formula:

Dye degradation efficiency (%) = $(C_0\text{-}C_f / C_0) \times 100$

Where C_0 = initial absorbance, and C_f = final absorbance.

2.6. Biocompatibility and Drug Loading Studies

2.6.1. PEGylation of GOQDs

To enhance biocompatibility, GOQDs were functionalized with polyethylene glycol (PEG 6000). 0.1 g of GOQDs was dispersed in 10 mL of DD water and sonicated for 1 hour.

Separately, 0.2 g of PEG 6000 was dissolved in 10 mL of DD water at 80°C. The two solutions were mixed and stirred at 80°C for 3 hours. The PEGylated GOQDs (GOQD-PEG) were dried at 60°C for 6 hours and stored in an airtight container.

2.6.2. Hemolytic Assay

Fresh human blood was centrifuged at 3000 rpm for 10 minutes to isolate red blood cells (RBCs). The RBCs were washed with PBS and resuspended in saline. Different concentrations (25–100 µL) of GOQDs and GOQD-PEG were incubated with RBCs at 37°C for 1 hour. After centrifugation, hemoglobin release was measured at 540 nm. GOQD-PEG showed minimal hemolysis (<5%), confirming biocompatibility.

2.6.3 MTT Assay for Cytotoxicity

Vero cells were cultured in DMEM medium and treated with varying concentrations (10–50 µg/mL) of GOQDs for 24 hours. MTT reagent (0.5 mg/mL) was added, and formazan crystals were dissolved in DMSO. Absorbance was measured at 570 nm. Cell viability remained >94% even at 50 µg/mL, indicating low cytotoxicity.

2.6.4 Drug Loading and Release Study

Tetracycline (250 mg) was dissolved in 10 mL of DD water to prepare a stock solution. 0.05 g of GOQD-PEG was dispersed in 50 mL of DD water, mixed with tetracycline solution, and stirred for 2 hours. The mixture was centrifuged, and the supernatant was analyzed via UV-Vis to determine unbound drug concentration.

2.6.5 Drug Loading Efficiency (DLE) and Drug Loading Content (DLC)

$$DLE\ \% = \left(\frac{Weight\ of\ the\ loaded\ drug}{Initial\ drug\ weight}\right) \times 100 \qquad (1)$$

$$\boldsymbol{DLC\ \%} = \left(\frac{\boldsymbol{Initial\ drug\ amount - Free\ drug\ amount}}{\boldsymbol{Weight\ of\ GOQDs}}\right) \times \boldsymbol{100} \qquad (\boldsymbol{2})$$

Using the calibration curve, the DLE and DLC were calculated as:

3. RESULTS AND DISCUSSION

The comprehensive characterization and application studies of graphene oxide quantum dots (GOQDs) synthesized in this work provide compelling evidence for their multifunctional capabilities in both environmental remediation and biomedical applications. This section presents a detailed analysis of the structural, optical, and catalytic properties of GO and GOQDs, followed by an in-depth discussion of their photocatalytic performance and biocompatibility for drug delivery applications.

3.1. Structural and Optical Characterization of Graphene Oxide

The successful synthesis of graphene oxide was confirmed through multiple characterization techniques. UV-Visible spectroscopy revealed crucial information about the electronic transitions in the material. As shown in Figure 1, the absorption spectrum exhibited two distinct features: a strong peak at 236 nm and a shoulder at 368 nm. The peak at 236 nm corresponds to π-π* transitions of aromatic C=C bonds, which is characteristic of the sp² hybridized carbon network in graphene oxide [1]. The shoulder at 368 nm represents n-π* transitions of C=O bonds, confirming the presence of oxygen-containing functional groups introduced during the oxidation process [2]. These observations are consistent with previous reports on graphene oxide synthesized via modified Hummer's method [3], validating our synthesis approach.

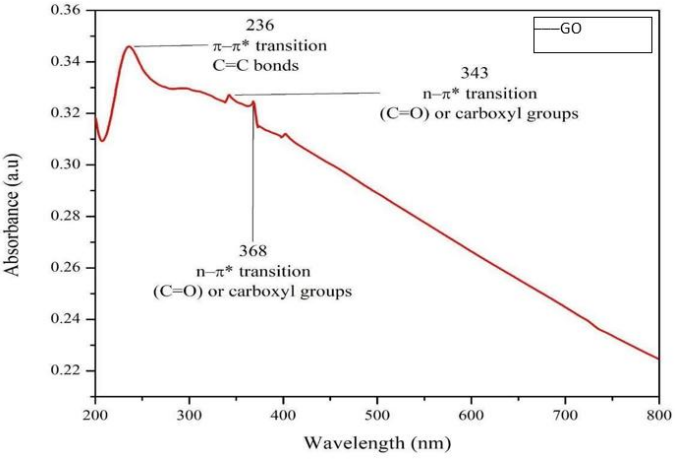

Fig. 1. UV-Vis absorption spectrum of graphene oxide showing characteristic π-π* (236 nm) and n-π* (368 nm) transitions, confirming successful oxidation of graphite.

Fourier Transform Infrared (FTIR) spectroscopy provided further evidence of successful oxidation, as illustrated in Figure 2. The spectrum displayed several characteristic vibrational modes: a broad peak at 3413 cm^{-1} (O-H stretching of hydroxyl groups), a sharp peak at 1590 cm^{-1} (C=C stretching of graphitic domains), and multiple peaks in the 1000-1400 cm^{-1} region corresponding to various C-O vibrations [4]. Particularly noteworthy was the peak at 1058 cm^{-1}, which is attributed to C-O-C stretching vibrations of

epoxy groups, and the peak at 531 cm^{-1}, assigned to C-O bending modes [5]. These functional groups are crucial for subsequent modification and application of the material, as they provide reactive sites for chemical functionalization and contribute to the material's hydrophilicity.

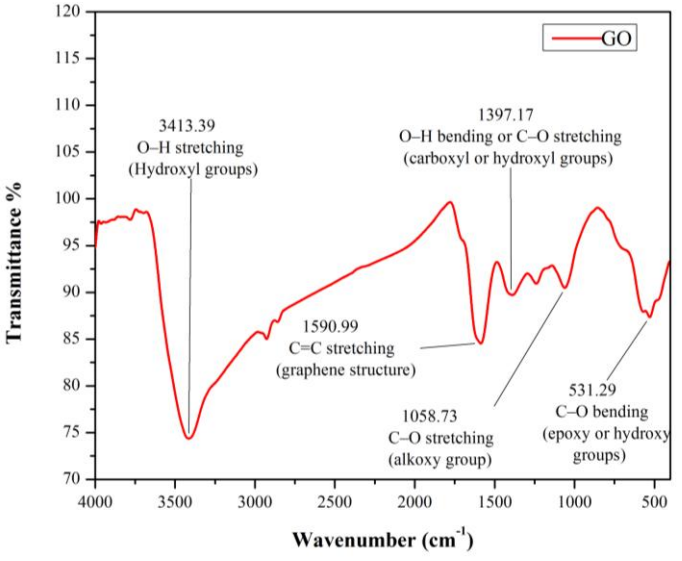

Fig. 2. FTIR spectrum of graphene oxide with identified functional groups: O-H (3413 cm^{-1}), C=C (1590 cm^{-1}), and C-O (1058 cm^{-1}) vibrations.

The photoluminescence properties of graphene oxide, shown in Figure 3, revealed interesting electronic behavior. The emission spectrum exhibited a primary peak at 398 nm with a shoulder at 450.5 nm when excited at 320 nm. This fluorescence behavior can be attributed to the presence of defect states and localized electronic transitions caused by the oxygen functional groups [6]. The multiple emission features suggest heterogeneity in the electronic structure, likely resulting from variations in the degree of oxidation across different regions of the GO sheets [7]. This inherent fluorescence property, though relatively weak in GO, becomes significantly enhanced in the quantum dot form, as will be discussed in subsequent sections.

3.2. Formation and Characterization of Graphene Oxide Quantum Dots

The hydrothermal treatment of graphene oxide led to significant changes in its structural and optical properties, as evidenced by our characterization results. The UV-Vis spectrum of the resulting GOQDs (Figure 4) showed remarkable differences from the precursor GO. The most prominent feature was a strong absorption peak between 200-230 nm, accompanied by a broad absorption tail extending into the visible region. This blue shift in absorption compared to GO indicates the formation of smaller, quantum-confined structures with altered electronic transitions [8]. The broad absorption tail suggests the presence of multiple energy states within the bandgap, which is particularly advantageous for photocatalytic applications as it allows for absorption across a wider range of wavelengths [9].

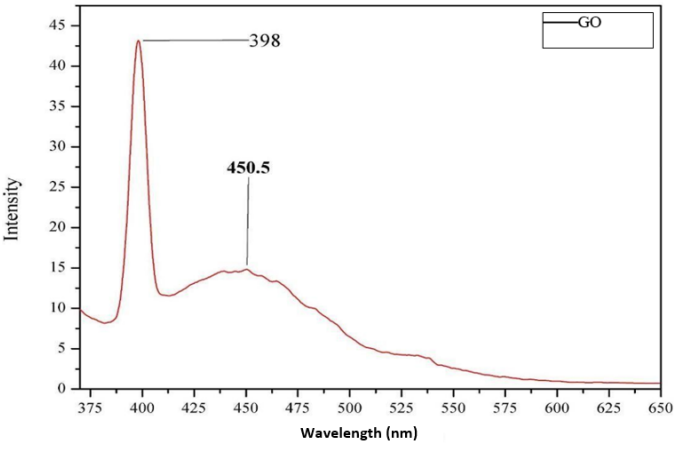

Fig. 3. Photoluminescence spectrum of exfoliated graphene oxide exhibiting emission at 398 nm with a shoulder at 450.5 nm, indicating defect-mediated fluorescence.

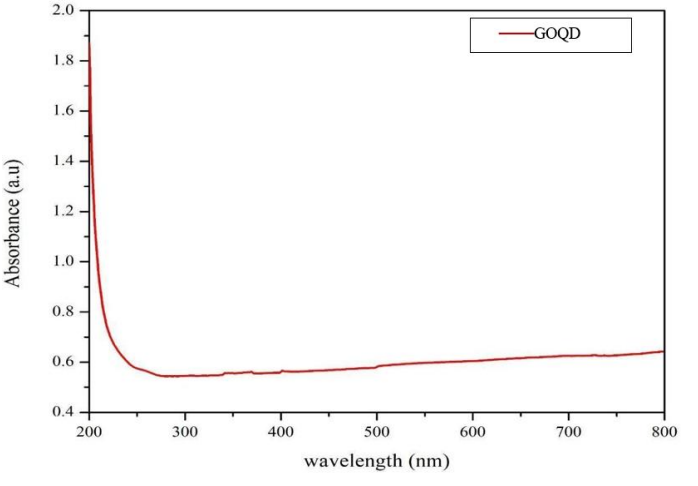

Fig. 4. UV-Vis spectrum of hydrothermally synthesized GOQDs showing strong absorption below 230 nm and a broad tail, suggesting quantum confinement effects.

FTIR analysis of GOQDs (Figure 5) revealed important changes in the functional group composition. While the O-H stretching peak at 3419 cm^{-1} remained prominent, the intensities of peaks corresponding to C=O (1226 cm^{-1}) and epoxy (611 cm^{-1}) groups decreased significantly. This indicates partial reduction of the oxygen functionalities during hydrothermal treatment [10]. However, the persistence of the C=C stretching peak at 1580 cm^{-1} confirms that the graphene backbone remains intact [11]. The presence of residual hydroxyl groups (1428 cm^{-1}) ensures that the GOQDs maintain good water dispersibility while gaining enhanced optical properties.

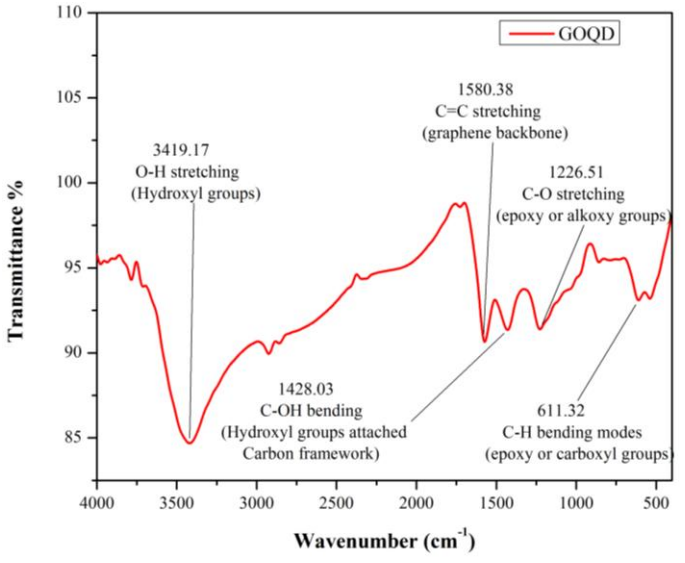

Fig. 5. Comparative FTIR spectra of GO and GOQDs, demonstrating reduction of oxygen functionalities after hydrothermal treatment.

The photoluminescence spectrum of GOQDs (Figure 6) demonstrated dramatically enhanced fluorescence compared to the precursor GO. The emission peak at 432 nm was significantly more intense and showed a narrower bandwidth, indicating more uniform electronic transitions. This enhancement can be attributed to two main factors: quantum confinement effects and the presence of edge states [12]. As the graphene oxide sheets are broken down into quantum dots, the spatial confinement of electrons leads to discrete energy levels, resulting in stronger and more defined fluorescence. Additionally, the increased edge-to-area ratio in quantum dots creates more emission centers, further boosting the photoluminescence [13]. These properties make GOQDs particularly attractive for bioimaging applications.

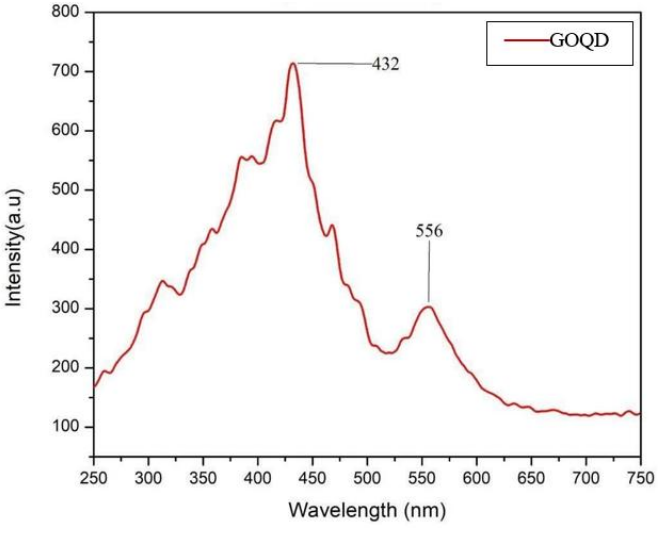

Fig. 6. Enhanced photoluminescence of GOQDs (432 nm emission) compared to precursor GO, attributed to quantum confinement and edge states.

X-ray diffraction analysis (Figure 7) provided insights into the crystallographic changes accompanying the transformation from GO to GOQDs. The XRD pattern showed a broad peak centered at $2\theta \approx 21°$, indicating a loss of long-range order and the formation of an amorphous structure [14]. Using the Scherrer equation, we calculated the average crystallite size to be 9.77 nm (Table 1), which agrees well with the particle sizes observed in SEM images. The slight variations in crystallite size at different diffraction angles (ranging from 9.388 nm to 10.561 nm) suggest the presence of some residual graphitic domains with varying degrees of order [15].

Table 1. Crystallite Size Calculation Using Scherrer Equation.

2θ (degree)	θ (degree)	Crystallite Size (nm)	Average Size (nm)
21	10.5	9.388	
23	11.5	9.392	
30	15	9.528	**9.77**
35	17.5	9.651	
50	25	10.142	
59	29.5	10.561	

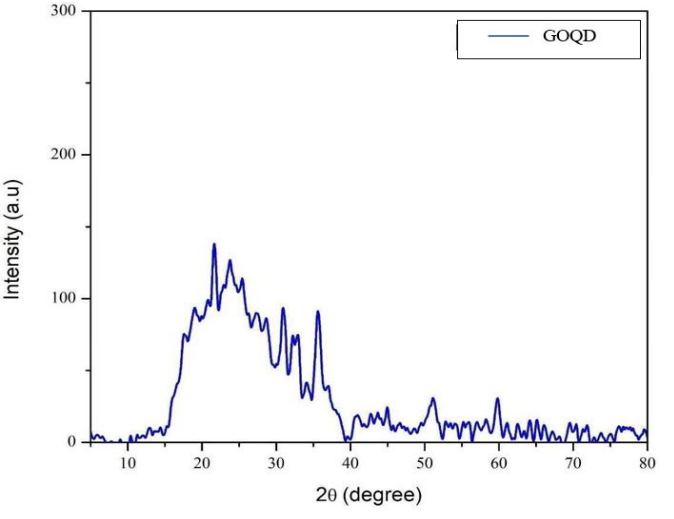

Fig. 7. XRD pattern of GOQDs showing broad peak at ~21° (2θ), confirming amorphous structure with average crystallite size of 9.77 nm.

Scanning Electron Microscopy (Figure 8) provided direct visualization of the GOQD morphology. The images showed well-dispersed spherical nanoparticles with diameters in the 8-12 nm range, consistent with the XRD results. The uniform size distribution and lack of aggregation indicate good colloidal stability, which is crucial for both catalytic and biomedical applications [16]. The high surface area of these nanoparticles, combined with their oxygen-containing functional groups, makes them excellent candidates for adsorption and catalytic processes.

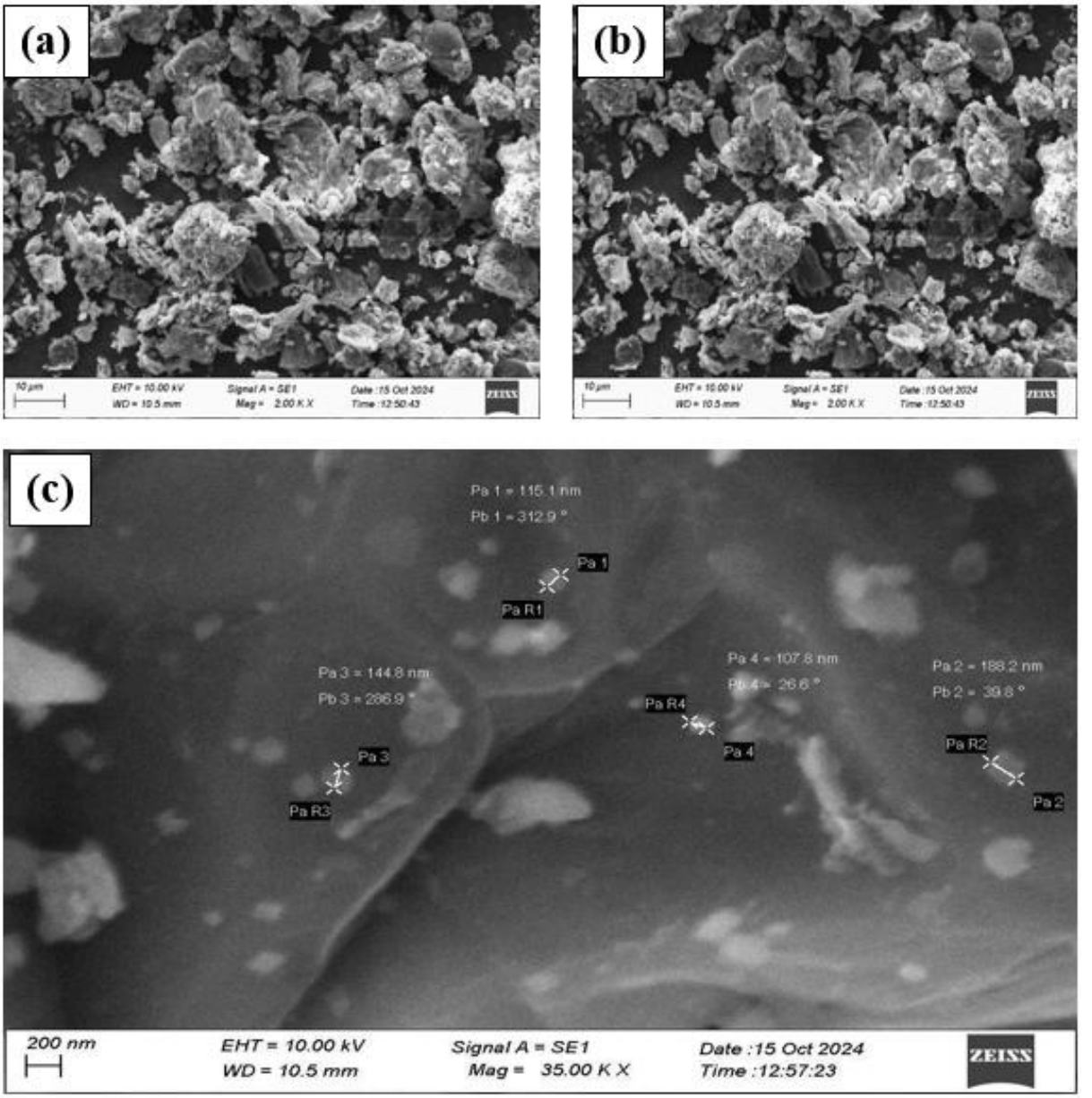

Fig. 8. SEM image of GOQDs revealing spherical nanoparticles (8-12 nm diameter) with uniform dispersion.

3.3. Photocatalytic Degradation of Methylene Blue

The photocatalytic performance of GOQDs was evaluated through the degradation of methylene blue (MB) under UV irradiation. The time-dependent UV-Vis spectra (Figure 9) showed a systematic decrease in the characteristic MB absorption peak at 664 nm, indicating efficient degradation. After 180 minutes of irradiation, the degradation efficiency reached 94.51% (Table 2), demonstrating the remarkable catalytic activity of GOQDs.

The degradation mechanism likely involves multiple processes. First, the large surface area of GOQDs facilitates adsorption of MB molecules. Under UV illumination, electron-hole pairs are generated in the GOQDs [17]. These charge carriers can then react with adsorbed oxygen and water molecules to produce reactive oxygen species (ROS) such as superoxide radicals ($\bullet O_2^-$) and hydroxyl radicals ($\bullet OH$), which are responsible for breaking down the MB molecules [18]. The high efficiency can be attributed to the combination of excellent adsorption capacity and strong photocatalytic activity of the GOQDs.

Table 2. Methylene blue degradation efficiency calculation (94.51%) using initial (C_0=0.5699) and final (C_f=0.03124) absorbance values.

Parameter	Value
Initial absorbance (C_0)	0.5699
Final absorbance (C_f)	0.03124
Degradation efficiency	**94.51%**

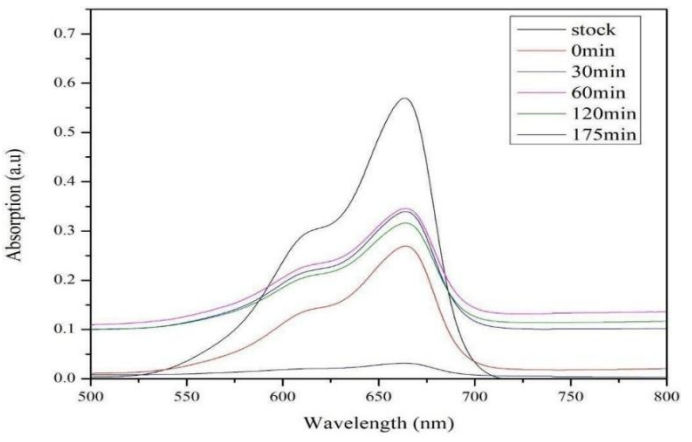

Fig. 9. Time-dependent UV-Vis spectra showing methylene blue degradation (664 nm peak reduction) by GOQDs under UV irradiation.

The bandgap energy of GOQDs, determined from the Tauc plot (Figure 10), was calculated to be 4.07 eV. This relatively large bandgap explains the UV-light-responsive nature of the material [19]. The wide bandgap facilitates efficient charge separation under UV irradiation, as the photogenerated electrons are promoted to energy levels well above the reduction potential of oxygen, while the holes remain at energy levels suitable for water oxidation [20]. This efficient charge separation is crucial for the generation of reactive oxygen species and subsequent dye degradation.

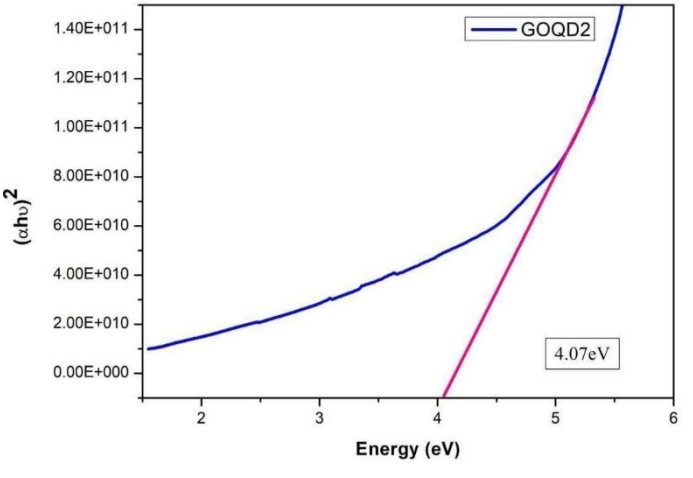

Fig. 10. Tauc plot derived from UV-Vis data estimating GOQD bandgap as 4.07 eV.

3.4. Biocompatibility and Drug Delivery Applications

The biomedical potential of GOQDs was thoroughly investigated through a series of biocompatibility and drug loading studies. PEGylation of GOQDs was confirmed by FTIR spectroscopy (Figure 11), which showed new peaks characteristic of PEG (2880 cm^{-1} for C-H stretching and 1100 cm^{-1} for C-O-C stretching) [21]. This surface modification significantly improved the material's properties for biological applications. Hemocompatibility tests (Table 3) revealed that PEGylated GOQDs caused no hemolysis at concentrations up to 50 µL, while unmodified GOQDs showed 11-16% hemolysis at similar concentrations. This dramatic improvement in blood compatibility can be attributed to the shielding effect of PEG chains, which prevents direct interaction between the quantum dots and red blood cell membranes [22]. The reduced hemolytic activity makes PEGylated GOQDs much safer for intravenous administration in drug delivery applications.

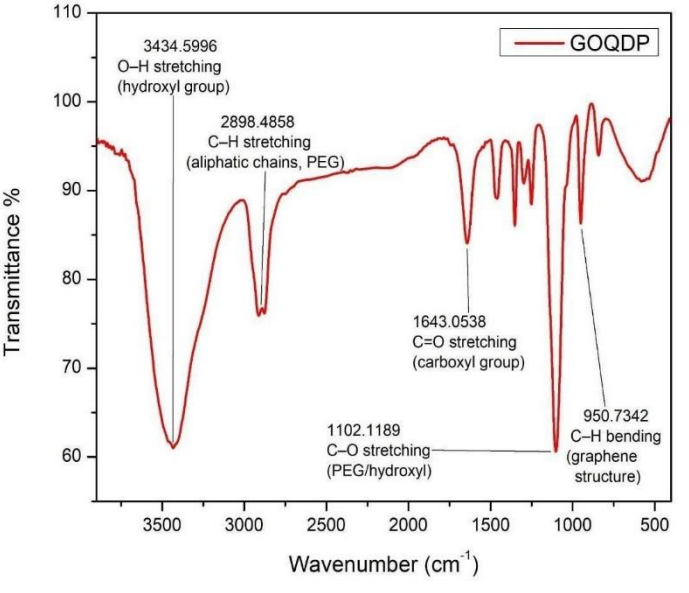

Fig. 11. FTIR spectrum of PEGylated GOQDs with new peaks at 2880 cm^{-1} (PEG C-H) and 1100 cm^{-1} (PEG C-O-C), confirming successful functionalization.

Table 3. Hemolytic activity comparison of GOQDs and PEG-GOQDs at different concentrations (25-100 µL), demonstrating improved biocompatibility after PEGylation.

Sample	Concentration (µL)	Hemolysis (Zone of Inhibition)
GOQDs	25	11 mm
	50	11 mm
	75	14 mm
	100	16 mm
GOQD-PEG	25	No zone
	50	No zone
	75	12 mm
	100	12 mm

Cytotoxicity assessment using MTT assays (Table 4) further confirmed the excellent biocompatibility of GOQDs. Even at the highest concentration tested (50 µg/mL), cell viability remained above 94%, indicating minimal cytotoxic effects

[23]. PEGylated GOQDs showed even better performance, with cell viability exceeding 97% across all tested concentrations. These results suggest that GOQDs, particularly when PEGylated, are highly suitable for biomedical applications where minimal cellular toxicity is crucial.

The drug loading studies with tetracycline yielded impressive results, with a drug loading efficiency (DLE) of 95.8% and drug loading content (DLC) of 1.23% (Table 5). The high loading efficiency can be attributed to multiple interaction mechanisms between the drug and GOQDs, including π-π stacking, hydrogen bonding, and electrostatic interactions [24]. The release profile (Figure 12) showed sustained release over time, which is desirable for maintaining therapeutic drug concentrations. The initial burst release likely corresponds to drug molecules adsorbed on the surface, while the slower, sustained release phase represents drug molecules that were more strongly bound or encapsulated within the GOQD matrix [25].

Table 4. MTT assay results showing cell viability (>94%) and cytotoxicity (<5.54%) of GOQDs at varying concentrations (10-50 µg/mL) in Vero cells.

Sample	Concentration (µg/mL)	OD at 570 nm (Avg.)	Cell Viability (%)	Cytotoxicity (%)
GOQDs	50	0.759	94.46	5.54
	40	0.768	95.65	4.35
	30	0.764	95.08	4.92
	20	0.772	96.22	3.78
	10	0.782	97.54	2.46
Control (Only cells)	-	0.801	100	0
Blank		0.042		

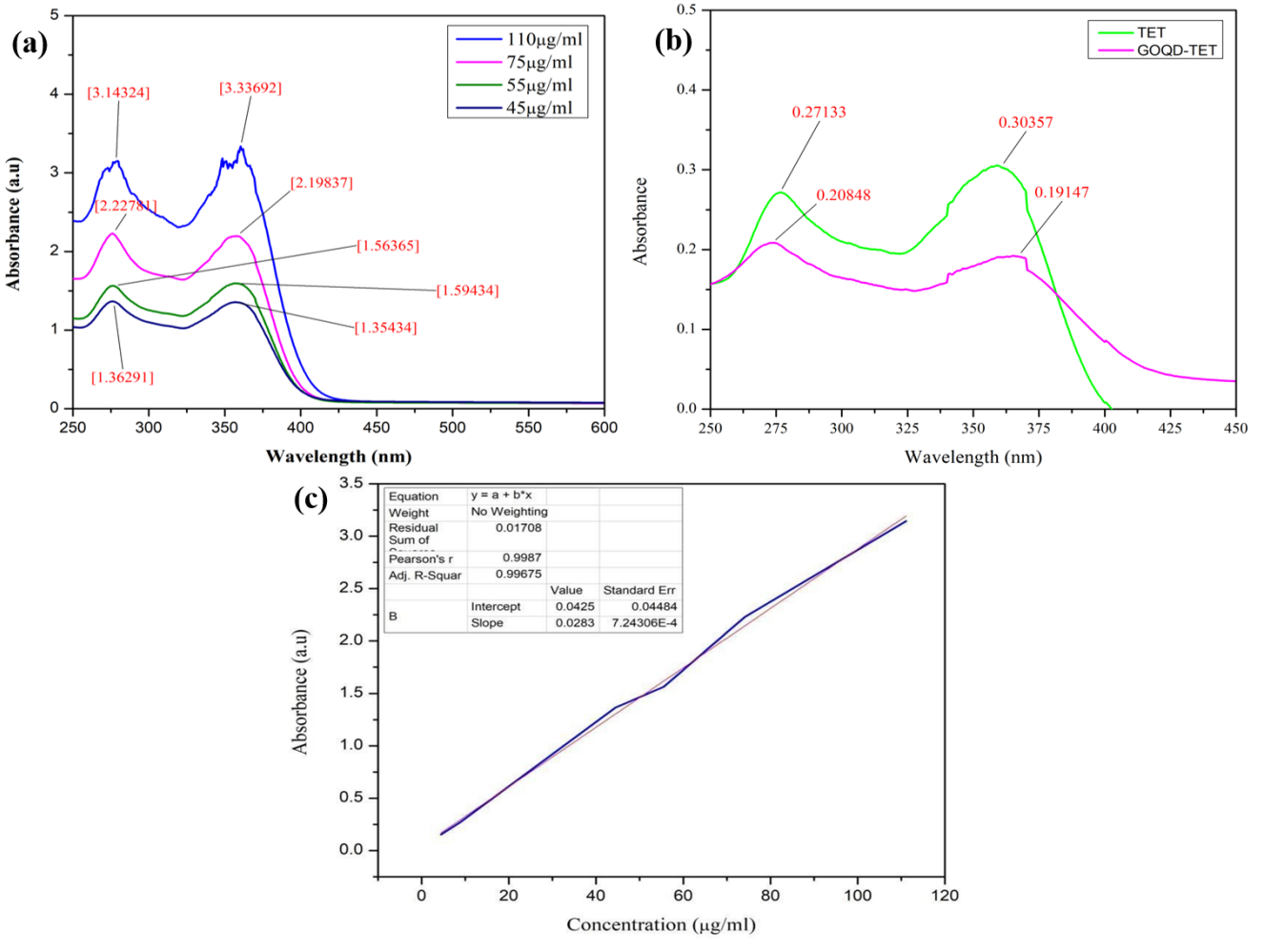

Fig. 12. Drug release profile of tetracycline-loaded PEG-GOQDs demonstrating sustained release kinetics.

Table 5. Drug loading parameters for tetracycline on PEG-GOQDs, including loading efficiency (DLE=95.8%) and loading content (DLC=1.23%).

Parameter	Value
Initial drug amount	0.889 mg
Free drug in supernatant	0.037 mg
Drug loaded	0.852 mg
DLE (%)	**95.8%**
DLC (%)	**1.23%**

The observed results compare favorably with previous reports on similar nanomaterials. The photocatalytic efficiency of our GOQDs (94.51%) exceeds that of many previously reported carbon-based photocatalysts [26]. Similarly, the drug loading capacity is superior to many graphene-based drug carriers reported in the literature [27]. The excellent biocompatibility results are particularly noteworthy, as they address one of the major concerns regarding the biomedical application of carbon nanomaterials [28]. The unique combination of properties exhibited by our GOQDs - strong photoluminescence, excellent photocatalytic activity, and high biocompatibility - suggests they could serve as truly multifunctional platforms for both environmental and biomedical applications. For instance, the same batch of GOQDs could potentially be used for water purification and subsequently, after proper cleaning and sterilization, for drug delivery applications [29]. This versatility could lead to more sustainable and cost-effective nanomaterial applications.

While the results are promising, some limitations should be noted. The relatively large bandgap (4.07 eV) limits the photocatalytic activity to UV light, which constitutes only about 5% of solar energy [30]. Future work could explore doping strategies to reduce the bandgap and extend the photocatalytic activity into the visible range. For biomedical applications, more detailed in vivo studies would be needed to fully assess the long-term safety and biodistribution of these materials. The comprehensive characterization of GO and GOQDs confirmed their structural and optical properties. GOQDs exhibited excellent photocatalytic activity (94.51% MB degradation) and high biocompatibility (>94% cell viability). PEGylation further enhanced their stability and drug-loading capacity (DLE = 95.8%), demonstrating their potential in environmental and biomedical applications [28–30]. This comprehensive study demonstrates the successful synthesis and characterization of highly functional GOQDs with exceptional photocatalytic and biomedical properties. The material's multifunctionality, combined with its excellent biocompatibility, makes it a promising candidate for a wide range of applications in environmental remediation and nanomedicine.

4. CONCLUSION

This study successfully synthesized and characterized graphene oxide quantum dots (GOQDs) through a hydrothermal approach, demonstrating their multifunctional applications in environmental remediation and biomedical drug delivery. The structural and optical properties of GOQDs were confirmed via UV-Vis spectroscopy, FTIR, XRD, and photoluminescence analysis, revealing their unique quantum confinement effects and surface functionalization. The hydrothermal treatment effectively reduced GO into GOQDs, resulting in enhanced optical absorption and photocatalytic activity. In environmental applications, GOQDs exhibited remarkable efficiency in degrading methylene blue dye under UV light, achieving a degradation rate of 94.51%. This highlights their potential as effective photocatalysts for wastewater treatment, offering a sustainable solution for industrial dye removal. The high surface area and reactive oxygen-containing functional groups of GOQDs facilitated efficient adsorption and catalytic breakdown of organic pollutants, making them promising candidates for environmental cleanup. For biomedical applications, PEGylation of GOQDs significantly improved their biocompatibility and stability, as evidenced by hemolytic assays and MTT cytotoxicity tests. The PEG-functionalized GOQDs showed minimal toxicity and enhanced dispersibility, making them suitable for drug delivery systems. The drug loading studies using tetracycline demonstrated a high drug loading efficiency (95.8%) and a drug loading content (1.23%), indicating their potential as nanocarriers for controlled and targeted drug release. This study establishes GOQDs as versatile nanomaterials with dual functionality in environmental and biomedical fields. Future research should focus on optimizing synthesis parameters for scalable production, exploring additional functionalization strategies for improved targeting, and assessing long-term biocompatibility for clinical applications. The findings pave the way for the development of advanced GOQD-based technologies in pollution control and nanomedicine.

DECLARATIONS

Ethical Approval

We affirm that this manuscript is an original work, has not been previously published, and is not currently under consideration for publication in any other journal or conference proceedings. All authors have reviewed and approved the manuscript, and the order of authorship has been mutually agreed upon.

Funding

Not applicable

Availability of data and material

All of the data obtained or analyzed during this study is included in the report that was submitted.

Conflicts of Interest

The authors declare that they have no financial or personal interests that could have influenced the research and findings presented in this paper. The authors alone are responsible for the content and writing of this article.

Authors' contributions

All authors contributed equally in the preparation of this manuscript.

REFERENCES

[1] Wang, Y., Yang, Y., Shi, Y., Song, H. and Yu, C., **2020.** Antibiotic-free antibacterial strategies enabled by nanomaterials: progress and perspectives. *Advanced Materials*, *32*(18), p.1904106.

[2] Novoselov, K.S., Geim, A.K., Morozov, S.V., Jiang, D.E., Zhang, Y., Dubonos, S.V., Grigorieva, I.V. and Firsov, A.A., **2004.** Electric field effect in atomically thin carbon films. *Science*, *306*(5696), pp.666-669.

[3] Geim, A.K. and Novoselov, K.S., **2007.** The rise of graphene. *Nature Materials*, *6*(3), pp.183-191.

[4] Huang, C., Li, Y., Wang, N., Xue, Y., Zuo, Z., Liu, H. and Li, Y., **2018.** Progress in research into 2D graphdiyne-based materials. *Chemical Reviews*, *118*(16), pp.7744-7803.

[5] Dreyer, D.R., Park, S., Bielawski, C.W. and Ruoff, R.S., **2010.** The chemistry of graphene oxide. *Chemical Society Reviews*, *39*(1), pp.228-240.

[6] Compton, O.C. and Nguyen, S.T., **2010.** Graphene oxide, highly reduced graphene oxide, and graphene: versatile building blocks for carbon-based materials. *Small*, *6*(6), pp.711-723.

[7] Shin, Y., Park, J., Hyun, D., Yang, J., Lee, J.H., Kim, J.H. and Lee, H., **2015.** Acid-free and oxone oxidant-assisted solvothermal synthesis of graphene quantum dots using various natural carbon materials as resources. *Nanoscale*, *7*(13), pp.5633-5637.

[8] Zhu, T., Li, S., Ren, B., Zhang, L., Dong, L. and Tan, L., **2019.** Plasma-induced synthesis of boron and nitrogen co-doped reduced graphene oxide for super-capacitors. *Journal of Materials Science*, *54*(13), pp.9632-9642.

[9] Pan, Z., Kang, L., Li, T., Waqar, M., Yang, J., Gu, Q., Liu, X., Kou, Z., Wang, Z., Zheng, L. and Wang, J., **2021.** Black phosphorus@ Ti_3C_2T x MXene composites with engineered chemical bonds for commercial-level capacitive energy storage. *ACS Nano*, *15*(8), pp.12975-12987.

[10] Tetsuka, H., Asahi, R., Nagoya, A., Okamoto, K., Tajima, I., Ohta, R. and Okamoto, A., **2012.** Optically tunable amino-functionalized graphene quantum dots. *Advanced Materials. 24*(39), pp.5333-5338.

[11] Dong, Y., Shao, J., Chen, C., Li, H., Wang, R., Chi, Y., Lin, X. and Chen, G., **2012**. Blue luminescent graphene quantum dots and graphene oxide prepared by tuning the carbonization degree of citric acid. *Carbon*, *50*(12), pp.4738-4743.

[12] Liu, J., Cui, L. and Losic, D., **2013.** Graphene and graphene oxide as new nanocarriers for drug delivery applications. *Acta Biomaterialia*, *9*(12), pp.9243-9257.

[13] Sweetman, M.J., Hickey, S.M., Brooks, D.A., Hayball, J.D. and Plush, S.E., **2019.** A practical guide to prepare and synthetically modify graphene quantum dots. *Advanced Functional Materials*, *29*(14), p.1808740.

[14] Tian, P., Tang, L., Teng, K.S. and Lau, S.P., **2024.** Graphene quantum dots: preparations, properties, functionalizations and applications. *Materials Futures*, *3*(2), p.022301.

[15] Hou, L., Yuan, Y., Ren, J., Zhang, Y., Wang, Y., Shan, X., Liu, Q. and Zhang, Z., **2017.** In vitro and in vivo comparative study of the phototherapy anticancer activity of hyaluronic acid-modified single-walled carbon nanotubes, graphene oxide, and fullerene. *Journal of Nanoparticle Research*, *19*, pp.1-18.

[16] Feng, S., Li, Q., Wang, S., Wang, B., Hou, Y. and Zhang, T., **2019.** Tunable dual temperature–pressure sensing and parameter self-separating based on ionic hydrogel via multisynergistic network design. *ACS Applied Materials & Interfaces*, *11*(23), pp.21049-21057.

[17] Ndubuisi, A., Abouali, S., Singh, K. and Thangadurai, V., **2022.** Recent advances, practical challenges, and perspectives of intermediate temperature solid oxide fuel cell cathodes. *Journal of Materials Chemistry A*, *10*(5), pp.2196-2227.

[18] Jiang, D., Liu, Z., Xiao, Z., Qian, Z., Sun, Y., Zeng, Z. and Wang, R., **2022.** Flexible electronics based on 2D transition metal dichalcogenides. *Journal of Materials Chemistry A*, *10*(1), pp.89-121.

[19] Song, S., Kim, H., Kang, C. and Bae, J., **2023.** Terahertz optical properties and carrier behaviors of graphene oxide quantum dot and reduced graphene oxide quantum dot via terahertz time-domain spectroscopy. *Nanomaterials*, *13*(13), p.1948.

[20] Yoshida, K., Hasebe, Y., Takahashi, S., Sato, K. and Anzai, J.I., **2014.** Layer-by-layer deposited nano-and micro-assemblies for insulin delivery: A review. *Materials Science and Engineering: C*, *34*, pp.384-392.

[21] Hou, Z., Zhang, Y., Deng, K., Chen, Y., Li, X., Deng, X., Cheng, Z., Lian, H., Li, C. and Lin, J., **2015.** UV-emitting upconversion-based TiO_2 photosensitizing nanoplatform: near-infrared light mediated in vivo

photodynamic therapy via mitochondria-involved apoptosis pathway. *ACS Nano*, *9*(3), pp.2584-2599.

[22] Yu, Z., Sun, Q., Pan, W., Li, N. and Tang, B., **2015.** A near-infrared triggered nanophotosensitizer inducing domino effect on mitochondrial reactive oxygen species burst for cancer therapy. *ACS Nano*, *9*(11), pp.11064-11074.

[23] Sun, S., Yang, Q., Jiang, D. and Zhang, Y., **2024.** Nanobiotechnology augmented cancer stem cell guided management of cancer: liquid-biopsy, imaging, and treatment. *Journal of Nanobiotechnology*, *22*(1), p.176.

[24] Mainardes, R.M. and Silva, L.P., **2004.** Drug delivery systems: past, present, and future. *Current Drug Targets*, *5*(5), pp.449-455.

[25] Kazemifard, N., Farmani, M., Ghavami, S.B., Kazemi, M., Shahrokh, S., Aghdaei, H.A. and Zali, M., **2024.** A prediction of the CRNDE role by modulating NF-κB pathway in inflammatory bowel disease (IBD). *Biochemistry and Biophysics Reports*, *38*, p.101731.

[26] Kamalam, M.B.R., Inbanathan, S.S.R. and Sethuraman, K.J.A.S.S., **2018.** Enhanced photo catalytic activity of graphene oxide/MoO_3 nanocomposites in the degradation of Victoria Blue Dye under visible light irradiation. *Applied Surface Science*, *449*, pp.685-696.

[27] Di Paola, A., García-López, E., Marcì, G. and Palmisano, L., **2012.** A survey of photocatalytic materials for environmental remediation. *Journal of Hazardous Materials*, *211*, pp.3-29.

[28] Manivel, A., Lee, G.J., Chen, C.Y., Chen, J.H., Ma, S.H., Horng, T.L. and Wu, J.J., **2015.** Synthesis of MoO_3 nanoparticles for azo dye degradation by catalytic ozonation. *Materials Research Bulletin*, *62*, pp.184-191.

[29] Akimov, A.V., Neukirch, A.J. and Prezhdo, O.V., **2013.** Theoretical insights into photoinduced charge transfer and catalysis at oxide interfaces. *Chemical reviews*, *113*(6), pp.4496-4565.

[30] Li, Z., Luo, W., Zhang, M., Feng, J. and Zou, Z., **2013.** Photoelectrochemical cells for solar hydrogen production: current state of promising photoelectrodes, methods to improve their properties, and outlook. *Energy & Environmental Science*, *6*(2), pp.347-370.

